Supporting Information

Pt Nanoparticles Loaded on Helical Chiral Carbon Nanotubes for Efficient Oxygen Reduction Reaction

Zhiping Li,‡ Jieling Zhang,‡ Zuozhong Liang,* Rui Cao*

Key Laboratory of Applied Surface and Colloid Chemistry, Ministry of Education, School of Chemistry and Chemical Engineering, Shaanxi Normal University, Xi'an 710119, China.

Correspondence E-mail: liangzuozhong@snnu.edu.cn, ruicao@snnu.edu.cn.

‡These authors contributed equally to this work.

Materials

Materials including L-glutamic acid (L-Glu), acetone, sodium hydroxide (NaOH), stearoyl chloride, ammonium persulfate, dihydrogen hex chloroplatinate hexahydrate (10 mg mL^{-1} $H_2PtCl_6 \cdot 6H_2O$), and perchloric acid ($HClO_4$), and solvents including ethanol and methanol were purchased from Energy Chemical. Commercial Pt/C (20 wt%) nanoparticles were purchased from Johnson Matthey Fuel Cells. Deionized water (DIW) was obtained from a Barnstead Nanopure water purification system. All chemicals were used as received without further purification.

Synthesis

Synthesis of chiral N-stearoyl-glutamate (C_{18}-L-Glu and C_{18}-DL-Glu)

First, 3.53 g of L-glutamic acid (L-Glu) was dissolved in a mixed solution consisting of deionized water (DIW, 14 mL), acetone (12 mL), and 1.92 g NaOH to maintain pH = 12. Subsequently, 6.05 g of stearoyl chloride and 10 mL of NaOH solution (0.2 mol L^{-1}) were slowly added to the above solution while continuously maintaining pH = 12 for 1 h. Hydrochloric acid was then added to the resulting solution to adjust the pH to 1, facilitating the formation of surfactant. The solid product was washed with DIW until pH = 7. After washing with petroleum ether and vacuum drying in a freeze dryer, C_{18}-L-Glu was obtained. C_{18}-DL-Glu was prepared using the same method as described above by replacing L-glutamic acid with DL-glutamic acid.

Synthesis of chiral carbon nanotubes (L-CCNT) and DL-CCNT

First, 0.0245 g of C_{18}-L-Glu was dissolved in 12.9 mL of methanol at room temperature and stirred for 30 min. Subsequently, 0.166 mL of pyrrole and 60 mL of DIW were added to the above solution. The resulting solution was stirred for 10 min, followed by the addition of a pre-cooled aqueous ammonium persulfate (APS) solution (0.548 g APS in 1.2 mL DIW). The resulting solution was stirred for another 30 min. After filtration, washing and drying, a black product was obtained and named helical polypyrroles (PPys)[1]. PPys were then pyrolyzed at 800 °C for 2 h under Ar atmosphere to obtain L-CCNT. DL-CCNT were prepared using the same method described above

by replacing C_{18}-L-Glu with C_{18}-DL-Glu. The yield of L-CCNT was about 0.075 g (yield 47%).

Synthesis of Pt-loaded carbon nanotubes (Pt@CNT, Pt@DL-CCNT, and Pt@L-CCNT)

First, 0.6 mL of $H_2PtCl_6 \cdot 6H_2O$ solution (concentration: 10 mg mL^{-1}) was added to 20 mL of deionized water along with 30 mg of the respective carbon nanotubes (m_{Pt}:$m_{Support}$ = 2:30). The mixture was ultrasonically dispersed at room temperature for 1 h to form a homogeneous solution. The mixed solution was then left standing for 3 h to allow the reaction system to reach equilibrium. Subsequently, the solvent was removed using a rotary evaporator, yielding a black solid powder. The obtained black solid powder was placed in a tube furnace and subjected to high-temperature calcination under an argon atmosphere. The temperature was raised to 800°C at a heating rate of 5 °C min^{-1} and held at that temperature for 2 h. After natural cooling, the final products Pt@CNT, Pt@DL-CCNT, and Pt@L-CCNT were obtained (0.026 g, yield 75%). By adjusting the amount of chloroplatinic acid hexahydrate added, Pt-based catalysts with different Pt contents can be obtained.

Characterization

Structures of materials were analyzed using an X-ray diffractometer (Bruker, D8 Advance). Morphologies of materials were obtained using a scanning electron microscope (SEM, Hitachi, SU8020) and a transmission electron microscope (TEM, JEOL, JEM-2100). X-ray photoelectron spectroscopy (XPS) results were measured with Kratos AXIS ULTRA XPS. Raman spectra were measured using a confocal laser micro-Raman spectrometer (LabRAM Odyssey). Zeta potentials were obtained by PALS Brookhaven Instruments at 1.02 V cm^{-1} and 20 revolutions. The content of metal Pt was measured with inductively coupled plasma-optical emission spectrometer (ICP-OES, Agilent 7800).

Electrochemical measurements

Electrochemical ORR measurements were conducted using a CHI 760E electrochemical analyzer coupled with a Pine modulated rotor flowmeter. The O_2-saturated 0.1 M $HClO_4$ was employed as the electrolyte. A rotating disk electrode

(RDE, 0.196 cm^2) served as the working electrode, while a carbon rod and a saturated Ag/AgCl electrode were used as the counter and reference electrodes, respectively. To prepare the catalyst ink, 2 mg of catalysts was dispersed in a mixture of 320 μL of isopropanol, 160 μL of water, and 20 μL of Nafion solution (5 wt%, DuPont), followed by ultrasonication for approximately 1 h to achieve a homogeneous slurry. Then, 20 μL of the resulting ink was deposited onto the RDE surface, yielding a catalyst loading of approximately 0.5 mg cm^{-2}, and allowed to dry under ambient conditions. Cyclic voltammetry (CV) measurements were performed at a scan rate of 5 mV s^{-1}. Linear sweep voltammetry (LSV) measurements were carried out at rotation speeds ranging from 400 to 1600 rpm. The Tafel slope was derived from LSV curve obtained at 2 mV s^{-1} and 1600 rpm. The controlled potential electrolysis was carried out at 0.56 V (versus reversible hydrogen electrode, vs RHE). The electron transfer number (n) was determined using a rotating ring-disk electrode (RRDE; disk area: 0.247 cm^2, ring area: 0.186 cm^2) based on LSV data acquired at 5 mV s^{-1}. The value of n was calculated according to Formula 1.

$$n = 4\frac{i_d}{i_d + i_r / N} \quad (1)$$

In the formula, i_d represents the disk current, i_r denotes the ring current, and N is the ring current collection efficiency (0.37). The hydrogen peroxide yield (%H_2O_2) was determined based on Formula 2.

$$\%H_2O_2 = 200\frac{i_r / N}{i_d + i_r / N} \quad (2)$$

The n can also be calculated according to the Koutecky-Levich (K-L) Formula 3.

$$\frac{1}{j} = \frac{1}{j_d} + \frac{1}{j_k} = B\omega^{-1/2} + \frac{1}{j_k} \quad (3)$$

Herein, j is the current density (mA cm^{-2}) measured in the experiment, j_d is the diffusion current density, j_k is the kinetic current density, ω is the rotation speed (rpm), and B can be calculated using the K-L formula 4.

$$B = 0.2nFC_0(D_0)^{2/3} / \nu^{-1/6} \quad (4)$$

Herein, n denotes the number of electrons transferred per oxygen molecule, F is the

Faraday constant (96485 C mol^{-1}), C_0 represents the bulk concentration of O_2 in O_2-saturated 0.1 M $HClO_4$ (1.2×10^{-6} mol cm^{-3}), D_0 is the diffusion coefficient of O_2 in the electrolyte (1.9×10^{-6} cm^2 s^{-1}), and v is the kinematic viscosity of the electrolyte (0.01 cm^2 s^{-1}).

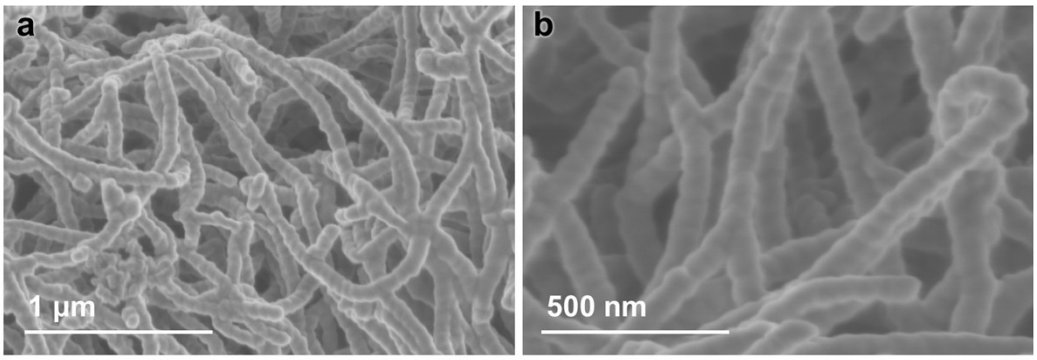

Fig. S1. SEM images of helical PPys.

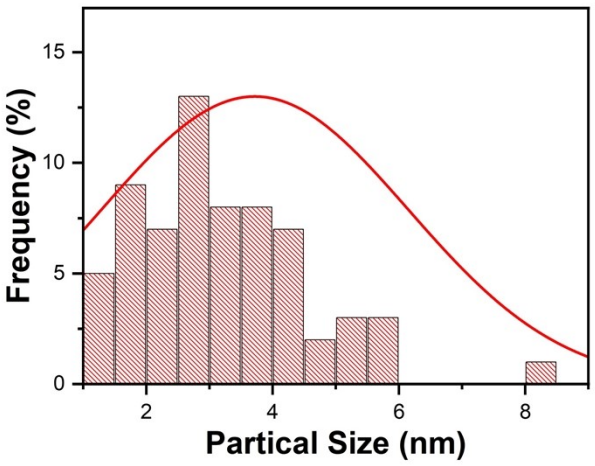

Fig. S2. Particle size distribution histogram image of Pt@CNT.

Fig. S3. Particle size distribution histogram image of Pt@DL-CCNT.

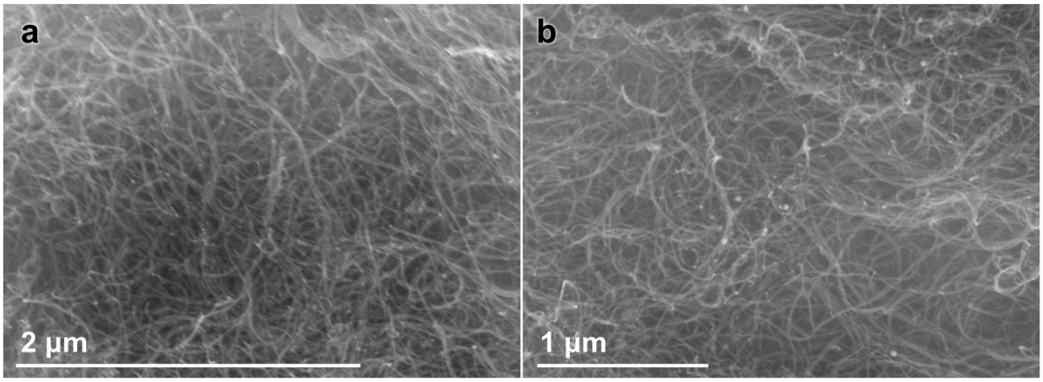

Fig. S4. SEM images of Pt@CNT (m_{Pt}:m_{CNT} = 1:30).

Fig. S5. SEM images of Pt@L-CCNT (m_{Pt}:$m_{L\text{-}CCNT}$ = 1:30).

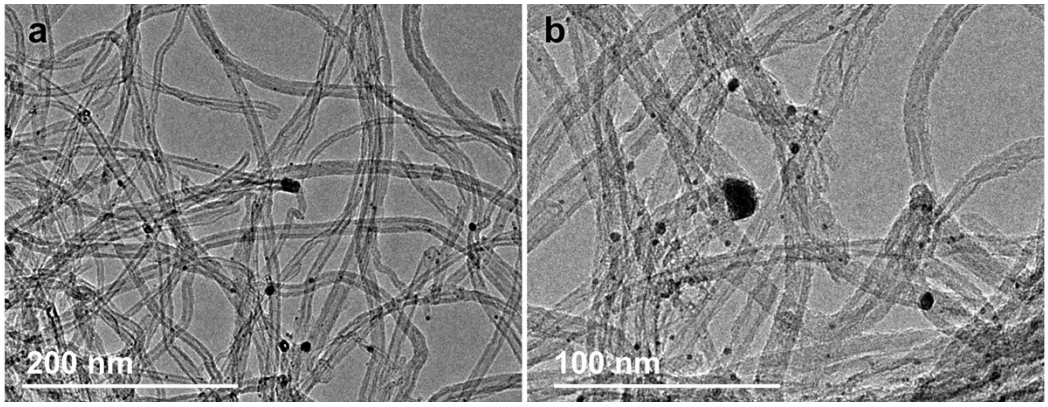

Fig. S6. TEM images of Pt@CNT (m_{Pt}:m_{CNT} = 1:30).

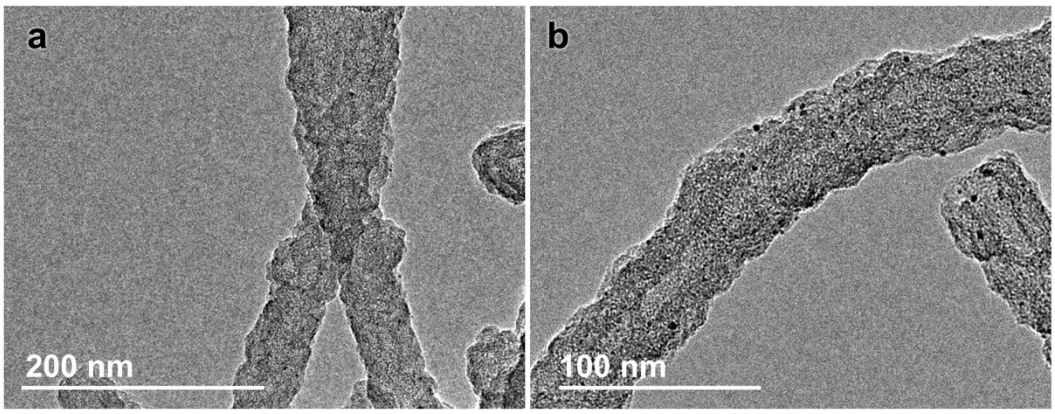

Fig. S7. TEM images of Pt@L-CCNT (m_{Pt}:$m_{L\text{-}CCNT}$ = 1:30).

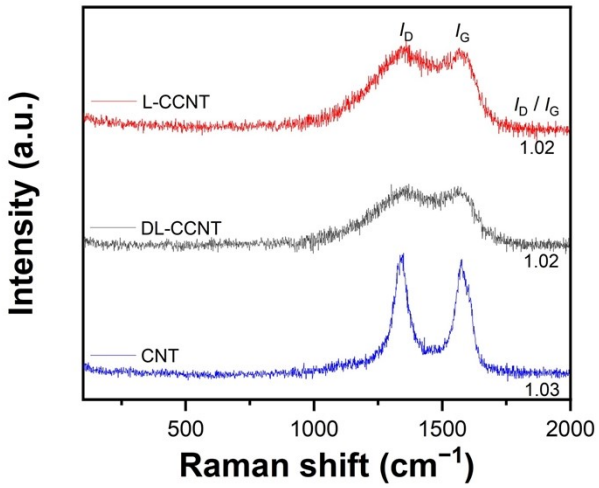

Fig. S8. Raman spectra of L-CCNT, DL-CCNT, and CNT.

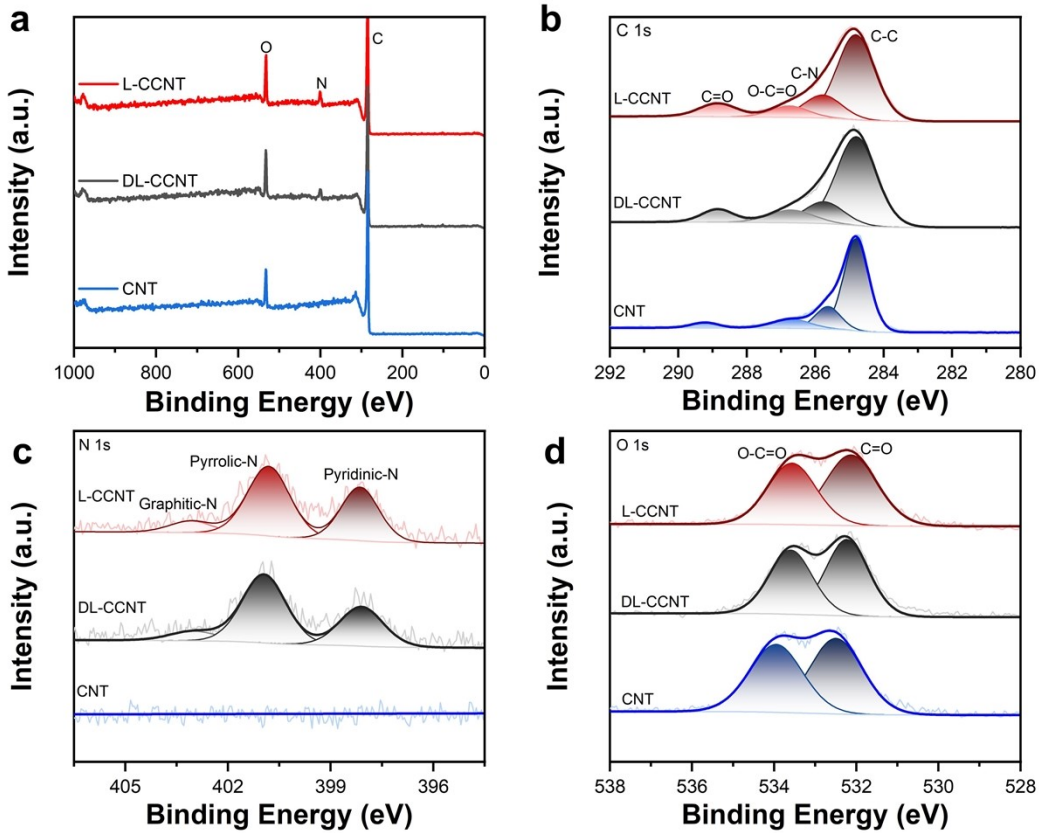

Fig. S9. (a) Full survey XPS spectra of L-CCNT, DL-CCNT, and CNT. XPS spectra of (b) C 1s, (c) N 1s, and (d) O 1s of L-CCNT, DL-CCNT, and CNT.

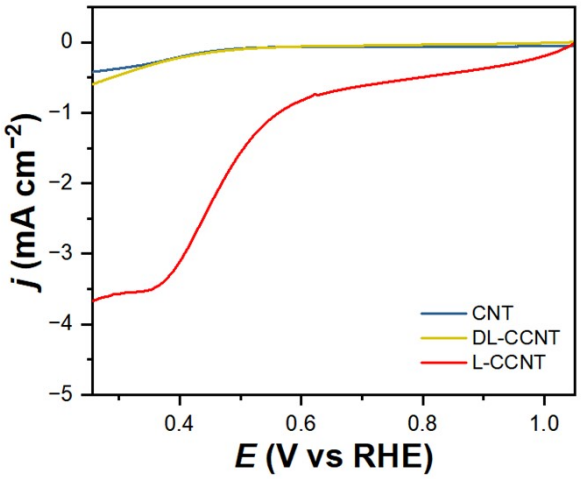

Fig. S10. LSV data for L-CCNT, DL-CCNT, and CNT in O_2-saturated 0.1 M $HClO_4$ solutions.

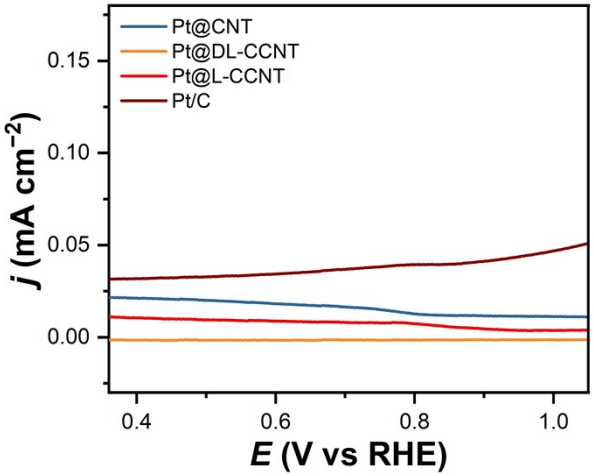

Fig. S11. Ring currents for Pt@L-CCNT, Pt@DL-CCNT, Pt@CNT, and Pt/C obtained in O_2-saturated 0.1 M $HClO_4$ solutions.

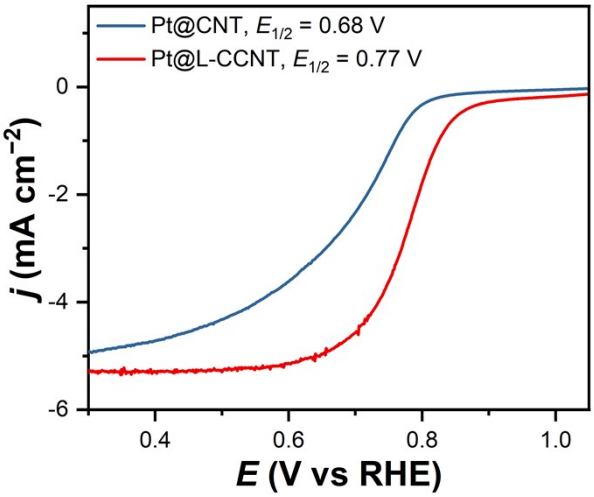

Fig. S12. LSV data of Pt@CNT and Pt@L-CCNT (m_{Pt}:$m_{CNT/L\text{-}CCNT}$ = 1:30) in O_2-saturated 0.1 M $HClO_4$ solutions.

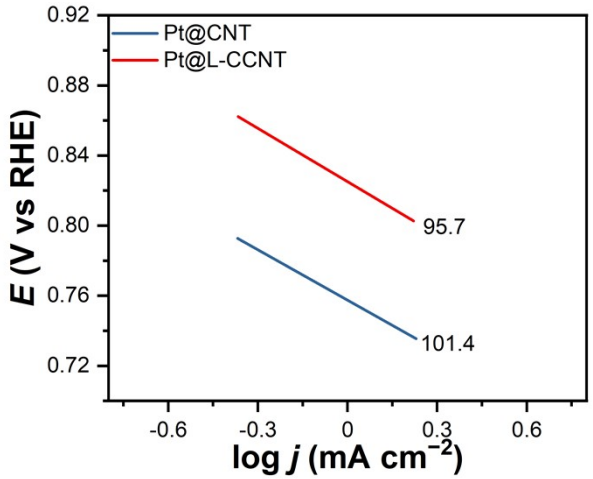

Fig. S13. Tafel slopes for Pt@CNT and Pt@L-CCNT (m_{Pt}:$m_{CNT/L\text{-}CCNT}$ = 1:30) in O_2-saturated 0.1 M $HClO_4$ solutions.

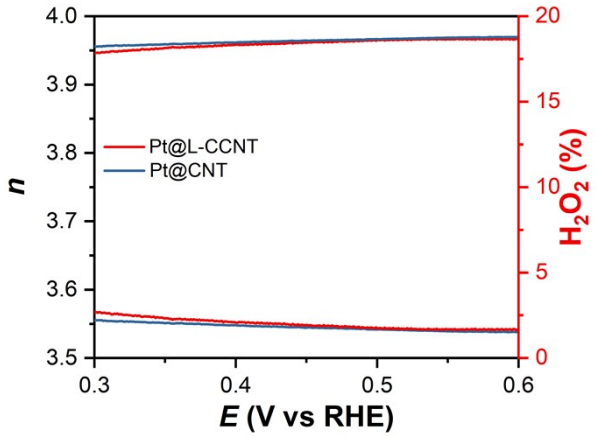

Fig. S14. Calculated *n* values and yield of H_2O_2 for Pt@CNT and Pt@L-CCNT (m_{Pt}:$m_{CNT/L\text{-}CCNT}$ = 1:30) in O_2-saturated 0.1 M $HClO_4$ solutions.

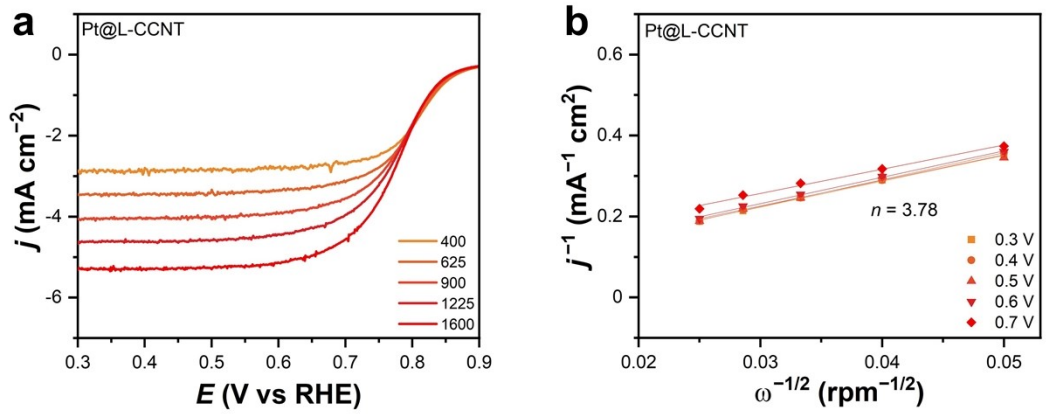

Fig. S15. (a) ORR LSV data at different rotation speeds and (b) K–L plots of Pt@L-CCNT (m_{Pt}:$m_{L\text{-}CCNT}$ = 1:30).

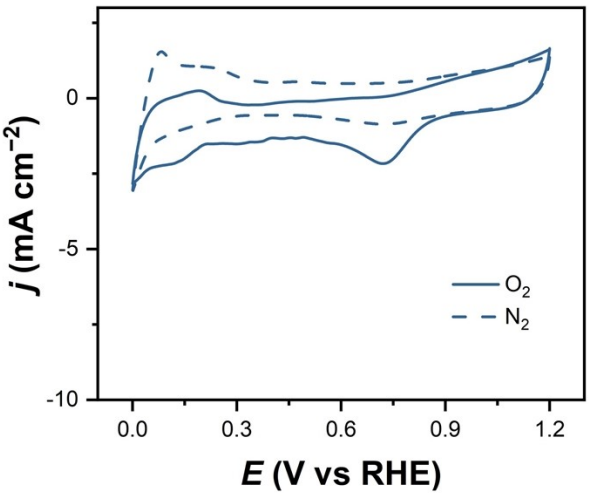

Fig. S16. CV data of Pt@CNT in N_2- and O_2-saturated 0.1 M $HClO_4$ solutions.

Fig. S17. CV data of Pt@DL-CCNT in N_2- and O_2-saturated 0.1 M $HClO_4$ solutions.

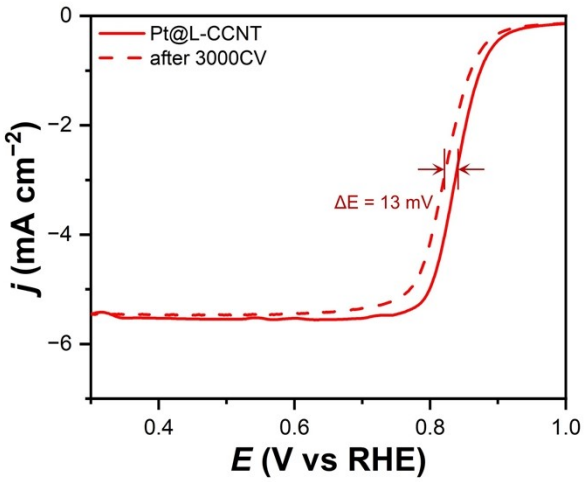

Fig. S18. LSV curves of Pt@L-CCNT before and after 3,000 cycles in O_2-saturated 0.1 M $HClO_4$ solutions.

Table S1. Comparison of the ORR performance of Pt-based catalysts and other catalysts.

Samples	**Pt (wt.%)**	$E_{1/2}$ **(vs RHE)**	**References**
Pt@L-CCNT	11.20	0.83 V	This work
Commercial Pt/C	20	0.83 V	This work
N-C/PtCo	19	0.90 V	2
Pt-NCNTs-1000	5.6	0.81 V	3
PtZn/NC	15.98	0.79 V	4
Pt/NPC	5.44	0.83 V	5
PtNi/NC	8.04	0.81 V	6
Pt_1Co_1/NC-Cl	1.76	0.84 V	7
PtZn-IMC@NC	12	0.85 V	8
CuCoNPC		0.72 V	9
Zn-N-P/NPC		0.80 V	10
Fe_1/DNC		0.82 V	11
Co-pCOF@MWCNT		0.72 V (0.1 M KOH)	12
CoMn@NCNT		0.82 V (0.1 M KOH)	13
Fe-NC@NCNT		0.88 V (0.1 M KOH)	14

Note: N-C (nitrogen-carbon); NCNTs (nitrogen-doped carbon nanotubes); NC (nitrogen-doped carbon); NPC (N-doped porous carbon); Pt_1Co_1/NC-Cl (axial Cl-coordinated Pt-Co dual atoms on N-doped graphitic carbon); PtZn-IMC@NC (N-doped carbon supported intermetallic PtZn); DNC (defect-containing nitrogen-doped carbon); MWCNT (multiwalled carbon nanotubes).

References

1. S. Liu, Y. Duan, X. Feng, J. Yang and S. Che, *Angew. Chem. Int. Ed.*, 2013, **52**, 6858-6862.
2. Z. Huang, Y. Wang, J. Xia, S. Hu, N. Chen, T. Ding, C. Zhan, C.-W. Pao, Z. Hu, W.-H. Huang, T. Shi, X. Meng, Y. Xu, L. Cao and X. Huang, *Sci. Adv.*, 2024, **10**, eadq6727.
3. H. Zhao, Y. Chen, H. Zuo, L. Li, L. Li, F. Ai, Z. Tang, T. Xing, Y. Zhang, L. Tao, Z. Tian, H. Yang, X. Geng and B. An, *Catal. Today*, 2024, **438**, 114811.
4. F. Fan, Y. Che, V. Efimov, K. Anton, S. Yan and T. Bian, *J. Electroanal. Chem.*, 2025, **998**, 119545.
5. Z.-Q. Xiao, X. Du, S. Ding, Z. Lyu, J.-X. An, P.-F. Xie, F. Wu, Y. Lin and J.-C. Li, *ACS Appl. Nano Mater.*, 2025, **8**, 9860-9867.
6. X. Chen, J. Guo, J. Liu, Z. Luo, X. Zhang, D. Qian, D. Sun-Waterhouse and G. I. N. Waterhouse, *J. Phys. Chem. Lett.*, 2023, **14**, 1740-1747.
7. Y. Zhang, F. Li, S. Li, Z. Zhang, Z. Sun, Y. Dou, R. Su, Y. Wu, L. Zhang, W. Chen, D. Wang and Y. Li, *Adv. Mater.*, 2025, **37**, 2507478.
8. P. Wang, K. Chen, J. Chen, G. Wang, W. Pan and Z. Wen, *Adv. Funct. Mater.*, 2024, **34**, 2408267.
9. H. Wang, X. Zhou, J. Su, Z. Liu, B. Xiao, L. Yang, J. Wang, Y. Li, X. Lu and X. Zhu, *Chem. Eng. J.*, 2025, **506**, 160020.
10. Y. Tan, Z. Zhang, F. Guo, S. Chen, H. Jiang, R. Chen, Z. Wang, Q. Chen, P. Yuan, S.-J. Bao, M. Xu and N. Cheng, *Adv. Mater.*, 2025, **37**, 2503254.

11. S. Ji, Y. Wang, H. Liu, X. Lu, C. Guo, S. Xin, J. H. Horton, F. Zhan, Y. Wang and Z. Li, *Adv. Funct. Mater.*, 2024, **34**, 2314621.

12. P. S. Thakur, V. Singh, V. Ganesan and M. Sankar, *Langmuir*, 2025, **41**, 10456-10468.

13. S. Qiang, J. Chen, S. Huang, H. Xu, X. Zhuo, H. Zhou, A. Yuan, H. Zhou and Y. Qiao, *J. Colloid Interface Sci.*, 2026, **701**, 138722.

14. Y. Shen, S. He, Y. Zhuang, S. Huang, C. Meng, A. Yuan, W. Miao and H. Zhou, *ACS Appl. Nano Mater.*, 2023, **6**, 16873-16881.